Changes in both top-down and bottom-up effective connectivity drive visual hallucinations in Parkinson's disease

George EC Thomas[1], Peter Zeidman[2], Tajwar Sultana[3,4,5], Angeliki Zarkali[1], Adeel Razi[3,6,7] & Rimona S Weil[1,2,8]

1. Dementia Research Centre, UCL Institute of Neurology, London, UK
2. Wellcome Centre for Human Neuroimaging, UCL, London, UK
3. Department of Computer and Information Systems Engineering, NED University of Engineering & Technology, Karachi
4. Department of Biomedical Engineering, NED University of Engineering & Technology, Karachi, Pakistan
5. Neurocomputation Laboratory, National Centre of Artificial Intelligence, Pakistan
6. Turner Institute for Brain and Mental Health, School of Psychological Sciences, Monash University, Clayton, Australia
7. CIFAR Azrieli Global Scholars Program, CIFAR, Toronto, Canada
8. Movement Disorders Consortium, UCL, London, UK

Corresponding author: Mr George EC Thomas, Dementia Research Centre, University College London, 8-11 Queen Square, WC1N 3AR, george.thomas.14@ucl.ac.uk

Abstract word count: 302

Main text word count: 5776

Display items: 1 table, 5 figures

References: 89

Supplementary materials: 2 figures, 1 methods file.

ABSTRACT

Visual hallucinations are common in Parkinson's disease and are associated with poorer quality of life and higher risk of dementia. An important and influential model that is widely accepted as an explanation for the mechanism of visual hallucinations in Parkinson's disease and other Lewy-body diseases is that these arise due to aberrant hierarchical processing, with impaired bottom-up integration of sensory information and overweighting of top-down perceptual priors within the visual system. This hypothesis has been driven by behavioural data and supported indirectly by observations derived from regional activation and correlational measures using neuroimaging. However, until now, there was no evidence from neuroimaging for differences in causal influences between brain regions measured in patients with Parkinson's hallucinations. This is in part because previous resting-state studies focus on functional connectivity, which is inherently undirected in nature and cannot test hypotheses about directionality of connectivity. Spectral dynamic causal modelling is a Bayesian framework that allows the inference of effective connectivity – defined as the directed (causal) influence that one region exerts on another region – from resting-state functional MRI data. In the current study, we utilise spectral dynamic causal modelling to estimate effective connectivity within the resting-state visual network in our cohort of 15 Parkinson's disease visual hallucinators, and 75 Parkinson's disease non-hallucinators. We find that visual hallucinators display decreased bottom-up effective connectivity from the lateral geniculate nucleus to primary visual cortex and increased top-down effective connectivity from left prefrontal cortex to primary visual cortex and medial thalamus, as compared to non-hallucinators. Importantly, we find that the pattern of effective connectivity is predictive of the presence of visual hallucinations and associated with their severity within the hallucinating group. This is the first study to provide evidence, using resting state effective connectivity, to support a model of aberrant hierarchical predictive processing as the mechanism for visual hallucinations in Parkinson's disease.

Keywords: Spectral dynamic causal modelling; resting-state functional MRI; Parkinson's disease; visual hallucinations; effective connectivity.

Abbreviations: CVA = canonical variates analysis; DCM = dynamic causal modelling; LGN = lateral geniculate nucleus; PEB = parametric empirical Bayes; PD-no-VH = Parkinson's disease without visual hallucinations; PD-VH = Parkinson's disease with visual hallucinations; PFC = prefrontal cortex; V1 = primary visual cortex; VH = visual hallucinations

INTRODUCTION

Visual hallucinations (VH) are common in Parkinson's disease, affecting up to 70% of patients[1]. Parkinson's disease patients who suffer from VH have a poorer quality of life[2], an increased rate of mortality[3], and are more likely to require nursing home care[4] and to develop subsequent dementia[5]. Until recently, models for how VH are generated within the brain remained somewhat limited and disparate, despite the high prevalence of VH and the clear burden they have on patients and their carers[6].

However, over the last few years, lines of evidence have converged on a predictive-coding framework that suggests the occurrence of VH relates to altered integration of sensory input (bottom-up information) and prior knowledge (top-down information, or a 'world model') within the visual system[7,8]. Patients with Parkinson's disease frequently have deficits in visual processing[6,9–12], with potentially greater deficits in higher-order visual processing in Parkinson's patients who hallucinate compared with those that do not[13]. Behavioural evidence has pointed specifically to impaired bottom-up accumulation of sensory evidence in visual hallucinators as compared to non-hallucinators[14], and patients with Lewy-body related VH have been shown to rely more strongly on top-down perceptual priors[15]. Notably, dorsolateral regions of prefrontal cortex are thought to play a key role in controlling top-down causal prediction error signalling[16,17].

Several key brain regions have been implicated in Parkinson's hallucinations. The thalamus is expected to be important in this framework as the synchronised functioning of these systems during normal visual perception relies strongly on thalamocortical connections[18,19]. Previous work has shown that Parkinson's disease hallucinators have reduced fibre cross section in white matter tracts connected to the medial thalamus early in disease course, with this spreading to almost the whole thalamus in later disease[20]. Additionally, lesion network mapping has revealed that a network centred on the lateral geniculate nucleus is consistently affected in studies of Parkinson's hallucinations[21] and in patients with brain lesions causing visual hallucinations[22].

Evidence also points towards the hippocampus as being important for application of perceptual priors due to its role in the encoding and retrieval of event-related memories[23] as

well as the integration of spatial and non-spatial contextual information[24]. In Parkinson's disease, VH have been linked to a higher burden of Lewy-related pathology in medial temporal lobes[13,25]. Alterations in functional connectivity to the hippocampus is seen in Parkinson's hallucinators, with increased functional connectivity to default mode and frontal regions, and decreased functional connectivity with the occipital cortex [26].

Primary visual cortex and frontal regions have been implicated in numerous functional MRI studies of Parkinson's hallucinators[27]. During exposure to simple visual stimuli, decreased activation in the primary visual and occipital cortex[28–30], has frequently been observed alongside increased activation in frontal[28,30] and visual association regions[29] in visual hallucinators. Exposure to complex visual stimuli in Parkinson's disease with VH is associated with decreased frontal cortical activation[31,32] and with altered functional connectivity in and between the attentional and default mode networks[33].

Altered functional connectivity has also been reported in resting-state analyses comparing Parkinson's disease visual hallucinators with non-hallucinators[27]. Studies looking at the default mode network have found mostly increased functional connectivity in hallucinators compared to non-hallucinators, including in frontal-parietal regions[34,35]. Increased connectivity within and between the default mode and attentional networks has also been found to correlate with performance on a complex visual task[36]. Hallucination severity is associated with strengthened stability of the default mode network[37], and greater mind wandering in visual hallucinators linked with increased functional connectivity between primary visual cortex and the dorsal default mode network[38].

Outside of the default mode network, increased occipital functional connectivity has been described with frontal and cortico-striatal regions[39] and decreased functional connectivity has been reported between the posterior cingulate cortex and parietal, temporal and occipital regions[40] in Parkinson's disease with VH.

Whilst these studies confirm altered connectivity and activation within visual network regions relating to VH in Parkinson's disease, these studies only examine differences in functional connectivity, which is a measure of the statistical dependencies or correlations between neuroimaging timeseries. The correlational, undirected nature of functional connectivity precludes any assessment of the *causal* influences of distinct brain regions and cannot provide a mechanistic explanation of neural mechanisms of Parkinson's hallucinations

based on hierarchical predictive processing which requires information on directionality to address the question of relative importance of bottom-up and top-down signalling.

Here, we employ dynamic causal modelling - a Bayesian framework that allows us to infer effective connectivity, which is designated as the directed (causal) influences among brain regions [41]. A dynamic causal model (DCM) is defined by a forward model that generates neuroimaging timeseries based on the underlying causes, controlled by the model parameters. These parameters represent quantities such as connection strengths between regions, and fall into three categories: neuronal parameters, haemodynamic parameters and parameters due to noise or measurement error[42]. Once a DCM is specified, data can be simulated under different variations of the model (for example with different connection strengths or architectures) to determine which model best characterises the observed data. Hypotheses within or between subjects can then be tested by comparing the evidence for different models.

When modelling resting state functional MRI data, the DCM methodology can become computationally intensive, due to the need to estimate random fluctuations in neuronal states[43]. Spectral DCM[41] has the advantage over conventional DCM when applied to resting state data, in that rather than modelling time-varying fluctuations in neuronal states, it models their second-order statistics or cross-spectra. This essentially models the dynamics of different brain regions in the frequency domain rather than the time domain. In doing so, it eliminates the need to estimate random neuronal fluctuations and is therefore more computationally efficient[44]. Additionally, it provides a reliable estimation of between region influences as well as enabling the accurate detection of group differences in effective connectivity.

In the current study, we use spectral dynamic causal modelling to estimate effective connectivity within a set of pre-defined visual brain regions in Parkinson's disease patients with and without visual hallucinations. We investigate the importance of top-down and bottom-up connectivity in explaining the differences between these groups, as well as the relative contributions of different regions and hemispheric connections to provide information about the architecture of this connectivity. We hypothesised that the presence of VH would be associated with both reduced bottom-up and increased top-down connectivity within this network, and that the severity of hallucinations would be associated with the pattern of changes in connectivity.

METHODS

Participants

We recruited 100 patients with Parkinson's disease to our UK centre from affiliated clinics. Inclusion criteria were a diagnosis of Parkinson's disease within 10 years, no history of traumatic brain injury or other psychiatric or neurological disorders, no contraindication to MRI and no ophthalmic disease sufficient to significantly impair visual acuity. Patients with Parkinson's disease satisfied the Queen Square Brain Bank Criteria for Parkinson's disease[45] and did not suffer from dementia. The study was approved by the Queen Square Research Ethics Committee and all participants provided written informed consent.

All participants underwent detailed clinical assessments. Motor function was assessed using the MDS-UPDRS parts II and III[46]. Cognition was tested using the Montreal Cognitive Assessment (MoCA)[47]. LogMAR was used to assess visual acuity[48]. Sniffin' Sticks were used to assess smell[49]. The Hospital Anxiety and Depression Scale (HADS) was used to assess depression and anxiety[50] and the REM Sleep Behaviour Disorder Questionnaire (RBDSQ) to assess sleep[51]. Levodopa equivalent dose scores (LEDD) were calculated[52]. Participants continued their usual therapy (including levodopa) for all assessments.

Patients with Parkinson's disease were classified as hallucinators (PD-VH) if they scored >1 on Question 1.2 of the MDS-UPDRS. We used the University of Miami Parkinson's disease Hallucinations Questionnaire (UMPDHQ)[53] to quantify severity of hallucinations 16 patients with Parkinson's disease scored >1 and were classified as PD-VH, whilst 84 patients did not and were classified as non-hallucinators (PD-no-VH). None of the PD-no-VH had a history of previous hallucinations. Differences in demographics and clinical characteristics between groups were examined in MATLAB with independent sample t-tests for normally distributed continuous variables, Kruskal-Wallis tests for nonnormally distributed ones, and Fisher's exact tests for categorical variables. Lilliefors test was used to assess normality. See Table 1 for full participant demographics.

Imaging protocol and pre-processing

MRI measurements were performed on a Siemens Prisma-fit 3T MRI system using a 64-channel receive array coil (Siemens Healthcare, Erlangen, Germany). Resting-state functional MRI data consisting of gradient echo EPI scans were acquired with the following parameters: TR=70ms; TE=30ms; flip angle=90°; FOV=192×192; voxel size=3×3×2.5mm; 110 volumes; scan-time=6 minutes. During resting-state functional MRI, participants were instructed to lie

quietly with their eyes open and avoid falling asleep; this was confirmed by monitoring and post-scan debriefing. T1-weighted magnetization-prepared 3D rapid gradient-echo (MPRAGE) anatomical images were also acquired. Imaging for all participants was performed at the same time of day (early afternoon), with participants receiving their normal medications.

Quality of resting-state functional MRI data was assessed using the MRI Quality Control tool[54]. As resting-state functional MRI can be particularly susceptible to motion effects, stringent exclusion criteria were adopted[55]. Specifically, participants were excluded if they met any of these criteria: (1) mean framewise displacement >0.3 mm, (2) any framewise displacement >5 mm, or (3) outliers >30% of the whole sample. This led to 10 participants being excluded (1 PD-VH and 9 PD-no-VH), resulting in 90 patients being included in the fMRI analysis, of which 15 were PD-VH and 75 were PD-no-VH.

Resting state data underwent standard pre-processing using SPM12. The first 5 volumes were discarded to allow for steady-state equilibrium. Functional data were spatially realigned, unwarped, normalized to MNI space using subject MPRAGE images and smoothed using a 6mm (FWHM) Gaussian kernel. Data were then denoised using ICA-based automatic removal of artifacts (ICA-AROMA)[56] which provides enhanced reproducibility of resting-state network, reduced loss of temporal degree of freedom and better conservation of signal of interest as compared to alternative noise removal strategies[57]. ICA-AROMA uses four features to classify motion components which are maximum realignment parameter correlation, edge fraction, CSF fraction and high frequency content, then the ICs identified as noise components are removed from the data. We used non-aggressive settings to avoid the risk of the loss of good signal.

ROI timeseries extraction

We defined a visual network comprising the following eight regions: left and right lateral geniculate nucleus (LGN), medial thalamus, primary visual cortex (V1), left and right hippocampus, and left and right prefrontal cortex (PFC) (see Figure 1A). We included thalamic nodes in this network due to previous work showing widespread thalamic white matter tract reductions in PD-VH[20], as well as the likely importance of thalamocortical connections in synchronising top-down and bottom-up streams during normal visual processing[18,19]. The LGN and V1 were selected as they are the locations of the first two post-retinal synaptic junctions within the visual system. Changes in V1 activation have been

reported in PD-VH on multiple occasions[28–30] and lesion network mapping work has highlighted the LGN as the centre of overlapping networks associated with PD-VH[21]. We selected the hippocampus due to reports of high burden of Lewy-related pathology in this region[13,58] and previous work describing changes in functional connectivity of the hippocampus in Parkinson's disease with VH[26]. We selected a dorsolateral node in PFC due to this region's role in control of visual attention[59] and its association with (top-down) causal prediction error signal[16,17]. Finally, the medial thalamus was selected due to its role in modulating PFC activity[60], and because our work has shown that the medial thalamus specifically shows white matter reductions in early-stage PD-VH[20].

Using SPM12, the resting state data for each subject was modelled using a GLM containing a discrete cosine basis set with frequencies ranging from 0.0078 to 0.1 Hz. Data were high pass filtered to remove any slow frequency drifts (<0.0078 Hz) and an F-contrast was specified across the discrete cosine basis functions, producing a statistical parametric map (SPM) that identified regions exhibiting BOLD fluctuations within the frequency band specified.

Locations for the LGN (MNI coordinates left, right: -22 -29 -4, 21 -27 -4), medial thalamus (MNI coordinates midline: 0 -15 6) and hippocampus (MNI coordinates left, right: -25 -15 -20, 25 -13 -21) were determined by structurally segmenting the thalamus and hippocampus in MNI space using Bayesian algorithms[61,62] and calculating the centre of gravity for the relevant regional masks with FSL 6.0. Coordinates for V1 (MNI coordinates midline: 0 -83 2) were taken from a previous DCM study[63] and those for the PFC (MNI coordinates left, right: -38 33 16, 38 33 16) from a large-scale cortical functional connectivity study[64]. For each subject, timeseries were acquired by computing the principal eigenvariate of signals from spheres centred on voxels at the above coordinates (see Figure 1B). Sphere radii were 10mm for V1, 8mm for medial thalamus, hippocampus, PFC and 4mm for LGN. All ROIs were additionally masked with the brain masks generated by fMRI-prep for each subject.

Within-subject analysis

Effective connectivity was estimated using spectral DCM implemented in SPM12 (www.fil.ion.ucl.ac.uk/spm). For each participant, a fully connected first level (within-subject) generative model of their fMRI time series was specified, considering all possible connections among the eight ROIs. These models were then inverted using the variational Laplace scheme, which finds model parameters that optimize the trade-off between explaining the data and minimizing model complexity[65]. This is quantified by the log model

evidence, which in DCM is approximated by the free energy, which serves as the basis for comparing models. Spectral DCM significantly simplifies the model inversion by replacing the original timeseries with their second order cross-spectra, meaning time-invariant parameters, rather than time-variant parameters, can be estimated[41,44]. For inversion, we used default prior probability densities provided by SPM for the neural, haemodynamic, and state noise parameters. Further technical detail on spectral DCM can be found in the supplementary methods.

Group level analysis

Parametric empirical Bayes

Once optimal within-subject parameters, including connection strengths, were estimated, these were taken to the group level. Here, individual differences were modelled as hypothesised group-level effects using parametric empirical Bayes (PEB)[66]. In this hierarchical framework, constraints on the posterior density of model parameters at a given level are enforced by the level above. This analysis differs from hierarchical linear regression modelling in a frequentist setting, in that the full posterior probability densities over the parameters (their expected values and covariance) are conveyed between levels and are used to inform the results. We modelled the following in the group-level design matrix; group mean, presence of VH, age and sex. All results were thus adjusted for age and sex within the PEB model. Default prior probability densities provided by SPM12 were used for the group-level neural parameters. Further technical detail on PEB can be found in the supplementary methods.

Hypothesis-based analysis

We investigated the relative contribution of top-down and bottom-up connections, inter- and intra-hemispheric connections as well as the involvement of different regions to the differences between subjects due to presence of VH. To do so, we designed a set of pre-defined hypotheses in the form of reduced GLMs with certain combinations of connection parameters switched off (i.e., prior expectation set to zero) to frame each hypothesis. These candidate models formed three experimental factors (see Figure 2). The first factor contained three families as follows: 1) bottom-up connections off, 2) top-down connections off, and 3) neither top-down nor bottom-up connections off. Top-down and bottom-up connections were defined based on the following hierarchy (from lower- to higher-level): LGN < V1 <

hippocampus < medial thalamus < PFC. The second factor contained three families: 1) intra-hemispheric connections off, 2) inter-hemispheric connections off, and 3) neither inter- nor intra-hemispheric connections off. The third factor contained 29 families resulting from the 32 possible subsets of five (2^5 = 32) bilateral regions (LGN, medial thalamus, V1, hippocampus and PFC), with the null and duplicate models removed. Combination across these factors gave 3x3x29 = 261 possible models, and 179 after removal of duplicate models and addition of a null model with no connections switched on. This resulted in a final factorial model space of 179^2 = 32041 reduced GLMs, with 179 possible models to explain the commonalities across participants and 179 possible models to explain the differences between participants due to the presence of VH. Using Bayesian model comparison, the evidence for each individual model, as well as the pooled evidence across the families within each factor, was assessed. To obtain numerical estimates for each connection parameter, Bayesian model averaging[67] was used to average parameter values across all models (weighted by the models' posterior probability). Only parameters with >95% posterior probability of being present vs. absent are reported.

Automatic parameter search

To test the validity of the network structure suggested by our hypothesis-based analysis, we additionally used a data-driven approach in the form of an automatic (greedy) search over connection parameters. This algorithm automatically switched off connection parameters from the full model until there was no increase in free energy[68,69]. The parameter values from the 256 models from the final iteration of the algorithm were averaged, weighted by their model evidence (Bayesian model averaging). Only parameters with >95% posterior probability of being present vs absent are reported. BrainNet Viewer was used to visualize data on cortical surfaces (https://www.nitrc.org/projects/bnv/)[70].

Leave-one-out cross validation

We next investigated whether subjects' group membership (PD-VH or PD-no-VH) could be predicted from their connectivity parameters, i.e., whether changes in effective connectivity between subjects were predictive of the presence of VH. We applied leave-one-out cross validation across all subjects, fitting a PEB model to all but one participant each time, and predicting the group effect for the left-out subject based on their individual connectivity parameters. Across subjects, we used the five connections that showed the greatest difference between PD-VH and PD-no-VH at group level as identified by the Bayesian model average

over our factorial model space (see Figure 4B). These were (in descending order): left LGN to V1, left PFC to V1, right PFC to V1, left LGN to left PFC, left PFC to medial thalamus. To ensure that our findings were not dependant on a specific number of connections, we also replicated our results using the top 10 connection strengths and the single largest connection strength.

Canonical variate analysis

Finally, we investigated whether, within the PD-VH group, hallucination severity (as measured by the UMPDHQ hallucinations severity scale) was associated with the pattern of effective connectivity seen. To do so, we applied canonical variate analysis (CVA), to model the effect of the same five connection strengths described above against UMPDHQ score for the 15 PD-VH subjects. CVA allowed dimension reduction of the five parameters into two canonical variates of connectivity. We tested the correlation between the first canonical variate of connectivity and the first canonical variate of hallucination severity, adjusted for age and sex. We replicated this analysis using the top 10 and the single largest connection strength.

RESULTS

Participants

Of the 90 PD patients in the current study, 15 were identified as having VH (PD-VH), while 75 had no VH (PD-no-VH). The PD-no-VH group had a higher female to male ratio than the PD-VH group (T=3.90, p=0.045), but there were no significant differences in the other demographics or clinical metrics, including no difference in measures of cognition or Levodopa equivalent dose (see Table 1).

Accuracy of DCM model estimation

The variance explained by DCM model estimation when fitted to the observed spectral data was 89.6±3.3% (mean ± standard deviation), with a range of 81.22% to 96.96%. This confirms the good fits of estimated DCM to the empirical cross-spectra. An example participant's estimation across spectral densities and estimated connectivity parameters can

be seen in Figure 1C-D. Cross-spectral density plots for all 15 PD-VH and a summary plot across all subjects can be seen in supplementary figure 1.

Measure	**PD-no-VH (N=75)**	**PD-VH (N=15)**	**Statistic**	***P***	
Sex (F:M)	45:31	4:11	T = 3.90	0.045	*
Age (years)	64.12 (7.78)	65.33 (8.75)	OR = -0.10	0.92	ns
Years of education	16.83 (2.73)	17.77 (3.59)	U = 3311	0.27	ns
MoCA (out of 30)	28.15 (2.08)	27.60 (1.76)	U = 3546	0.14	ns
UPDRS-III	21.89 (11.34)	25.40 (14.67)	U = 3331	0.38	ns
Bionocular LogMAR visual acuity	-0.09 (0.12)	-0.04 (0.34)	U = 3325	0.34	ns
HADS depression score	3.97 (2.95)	4.73 (3.43)	U = 3334	0.39	ns
HADS anxiety score	5.77 (3.80)	7.00 (4.38)	U = 3314	0.29	ns
RBDSQ score	3.96 (2.41)	5.13 (2.53)	U = 3255	0.08	ns
Smell test (Sniffin' Sticks)	7.92 (3.16)	6.40 (3.29)	T = 1.69	0.09	ns
Disease duration (years)	3.83 (2.38)	4.67 (2.35)	U = 3286	0.17	ns
Levodopa equivalent dose (mg)	431.89 (259.88)	421.67 (196.57)	U = 3389	0.80	ns

Table 1 – Participant demographics. Means (SDs) reported. MoCA = Montreal Cognitive Assessment. UPDRS = Unified Parkinson's Disease Rating Scale. HADS = Hospital Anxiety and Depression Scale. Binocular LogMAR: lower score is better visual acuity. RBDSQ = REM (Rapid Eye Movement) Sleep Behaviour Disorder Screening Questionnaire.
*P<0.05; ns = not significant

Commonalities of visual network effective connectivity across participants

The visual network architecture common to all participants with Parkinson's disease was defined by the commonalities in connection strengths, or group mean, identified in our

hypothesis-based analysis. Across all reduced GLMs, the highest associated posterior probability was 53% (Figure 3A). This GLM had its commonalities quantified by the effective connectivity parameters of model 172 (Figure 3C, left panel), which was the fully connected model (all connections switched on). Summing across all GLMs which had their commonalities parameters deployed according to this model, the posterior probability reached 99.8% (Figure 3B, upper panel). This strong evidence indicates that the commonalities across subjects were best explained by the fully connected model. Thus, no connections could be excluded without reducing the quality of the model. Accordingly, family-based analyses revealed that both top-down and bottom-up connections, (family 3 in factor 1, Figure 3D), both inter- and intra-hemispheric connections (family 3 in factor 2, Figure 3E), and connections to and from all regions (family 23 in factor 3, Figure 3F) were important in explaining the commonalities across subjects.

Bayesian parameter averaging of commonalities between subjects revealed that this fully connected model was characterised by strongly positive interhemispheric effective connectivity, and strongly positive intrinsic (self) connectivity in all regions except the PFC and medial thalamus. Note that effective connectivity with a positive sign represents excitatory influences, and negative sign represents inhibitory influences except for (log-scaled) self-connections which are always inhibitory by definition. Hence positive self-connections represent more inhibition and negative self-connections represent disinhibition. Other key features included generally negative afferent PFC connectivity, and positive connectivity to V1 from LGN and PFC (Figure 4A). This architecture was confirmed by our data-driven automatic search over parameters, which identified a highly connected network with very similar connection strengths (supplementary figure 2).

Effect of visual hallucinations on visual network architecture

The differences in visual network architecture in PD-VH compared to PD-no-VH were best explained by GLMs with parameters deployed according to model 143 (Figure 3A), with an associated summed posterior probability of 53% (Figure 3B bottom). This model was defined by the presence of both top-down and bottom-up intra-hemispheric connections to and from LGN and PFC (Figure 3C, right panel). Accordingly, family-based analysis revealed that both top-down and bottom-up connections, (family 3 in factor 1, Figure 3D), intra-hemispheric connections (family 2 in factor 2, Figure 3E), and connections to and from LGN

and PFC (family 17 in factor 3, Figure 3F) were the best explanation for differences between subjects due to presence of VH.

While model 143 had the strongest posterior probability across all 179 models, its overall probability was only 53%. There was therefore not a single best explanation for the differences in connectivity due to VH (i.e., a model with 95% probability or more[71,72]). This *dilution of evidence* effect is expected given the large number of models. Therefore, to summarise the estimated parameters across the 32041 models, while taking into account that different models had different levels of evidence, we performed Bayesian model averaging. We then thresholded the averaged parameters at >95% posterior probability, corresponding to strong evidence[71,72], for effects being present versus absent.

Bayesian model averaging across all models in the factorial model space revealed several key differences in effective connectivity in PD-VH compared to PD-no-VH. These included reduced effective connectivity from left LGN to V1 (0.20Hz) and medial thalamus (0.16Hz), increased effective connectivity from left LGN to left PFC (0.17Hz), increased effective connectivity from left PFC to medial thalamus (0.17Hz) and V1 (0.20Hz) and decreased effective connectivity from right PFC to V1 (0.18Hz). Additionally, in PD-VH, we observed increased self-inhibition in the right PFC and right hippocampus, and disinhibition of the left PFC, left hippocampus and left LGN. The full pattern of connectivity differences can be seen in Figure 4B. The differences between subjects due to the presence of VH identified after an automatic search over parameters were in concordance with those described above (supplementary figure 2).

This indicates that both increased top-down and reduced bottom-up effective connectivity is important in explaining the differences between PD-VH and PD-no-VH groups, particularly relating to the LGN and PFC, with a lateralised effect observed from the PFC.

Predicting group membership and hallucination severity

We used leave-one-out cross validation to test whether a participant's group membership (i.e., hallucination status) could be predicted from their individual connection strengths for the top five largest group differences, as previously descried in the Methods section. We found that 71 out of 90 subjects had their true group membership value within the estimated 90% credible interval, with 14 out of 15 PD-VH and 57 out of 75 PD-no-VH falling in this range. Predicted group membership correlated significantly with actual group membership (r

= 0.24, P = 0.012; Figure 5A). Additionally, this correlation remained significant when predicting group membership using the top 10 connections (r = 0.30, P = 0.002) or the single largest connection (r = 0.22, P = 0.012).

We next investigated whether hallucination severity within the PD-VH group was associated with the first canonical variate derived from five parameters described above. We found that this correlated significantly with the canonical variate derived from adjusted UMPDHQ score (r = 0.864, P = 0.008; Figure 5B), indicating that the pattern of connectivity within the visual network in the PD-VH group was predictive of hallucination severity. This association remained significant when using the top 10 connection strengths (r = 0.854, P=0.018) and approached significance when using the single largest connection (r = 0.643, P=0.053).

DISCUSSION

In the current study, we utilised spectral DCM for resting state functional MRI data to investigate visual network effective connectivity in Parkinson's disease patients with and without VH. We examined how effective connectivity differed between patients with and without VH, finding that a model comprising both reduced bottom-up and increased top-down effective connectivity best explained differences between patient groups, with differences in effective connectivity relating to severity of hallucinations. To our knowledge, this is the first study demonstrating changes in causal influences between brain regions in Parkinson's disease visual hallucinators.

The ability of DCM to non-invasively infer the directionality of influences between brain regions in living patients[73] ideally places it to investigate hypotheses relating to the hierarchical processing account of VH, where reduced bottom-up sensory processing is proposed to occur alongside overweighting of top-down perceptual priors[14,15]. Previous studies, while making valuable insights[27,74], have tended to look at functional connectivity changes, which are inherently undirected in nature[73], and so cannot directly test this hypothesis. We designed a factorial model space to specifically probe the relative contribution of top-down and bottom-up connections within the visual network in PD-VH versus PD-no-VH, and additionally tested inter- versus intra-hemispheric connectivity alongside regional involvement to estimate the architecture of any changes. Finally, we

assessed whether the pattern of visual network changes observed was associated with a clinically-relevant measure: the severity of hallucinations.

Our Bayesian model comparison across this model space revealed that the differences between subjects due to the presence of VH were explained best by a combination of both top-down and bottom-up effective connections. In particular, these were intra-hemispheric connections to and from the LGN and PFC. Bayesian model averaging across the model space revealed both the valence and magnitude of such changes. Among the largest were decreased effective connectivity in PD-VH from the left LGN to medial thalamus and V1, as well as increased effective connectivity from left PFC to medial thalamus and V1. Thus, some of the largest differences we found between PD-VH and PD-no-VH reflected both increased top-down and reduced bottom-up connections within the visual network, with regions at either end of the visual hierarchy (LGN and PFC) emerging as particularly important.

The single largest difference we found between PD-VH and PD-no-VH was decreased effective connectivity from left LGN to V1 in PD-VH. This is consistent with previous structural network mapping work, which found that coordinates of atrophy from studies of VH in Parkinson's disease were connected to a network centred on the LGN[21]. Similarly lesions in patients with visual hallucinations are connected to an LGN-centred functional network[22]. Task-based functional MRI work in PD-VH has also shown decreased activity in primary visual and occipital cortex fairly consistently in PD-VH compared to PD-no-VH[28–30]. Additionally, magnetic resonance spectroscopy has revealed reduced occipital GABA[75] and FDG-PET has revealed occipital glucose hypometabolism associated with VH in Parkinson's disease[76,77]. Reduced activity of early visual cortex would be consistent with reduced bottom-up input from LGN, although we did not find altered efferent connectivity from V1 in PD-VH. Interestingly, a recent study of effective connectivity in Parkinson's disease without VH found that modulation of LGN by the superior colliculus in response to luminance contrast changes was inhibited in Parkinson's disease compared to controls[78]. The way in which such stimuli modulate LGN and the superior colliculus may also change as a result of treatment[79].

We observed changes in effective connectivity to the medial thalamus in PD-VH, with decreased connectivity from the left LGN, and increased connectivity from left PFC. This is congruent with our recent work finding that thalamic tracts connected to the mediodorsal

thalamic nucleus had reduced fibre cross section in PD-VH[20], although these findings did not indicate the direction of information flow. Previous diffusion tensor imaging work revealed increased mean diffusivity in bilateral thalamic sub regions projecting to prefrontal and parieto-occipital cortices in Lewy body dementia patients with VH[80]. Additionally, a recent post-mortem study found that atrophy in the mediodorsal nucleus of the thalamus was significantly greater in Lewy body dementia patients with VH[81].

The thalamus is expected to play an important role in accounts of dysfunctional hierarchical predictive processing, due to its role in synchronising simultaneous streams of information (e.g. top-down and bottom-up) in normal visual processing[18,19]. This is corroborated by the changes in thalamic effective connectivity we found in PD-VH. Interactions between thalamus and prefrontal cortex are important in dealing with perceptual uncertainty during decision making[82]. Two separate pathways may exist for this, with low-signal-related uncertainty (as would be expected with reduced bottom-up sensory input) resolved by dopaminergic projections from medial thalamus that increase prefrontal output[83]. Interestingly, changes in thalamic resting state functional connectivity[84], as well as changes in thalamocortical effective connectivity[85] may also underlie hallucinations during exposure to LSD, consistent with a more general role for changes in thalamic connectivity in hallucinations in other contexts[86].

We also found increased top-down effective connectivity in PD-VH from left PFC to medial thalamus, and V1. This might help to explain previous task-based functional studies reporting increased activity in PD-VH prefrontal cortices in response to simple stimuli[28,30], although other work has shown that prefrontal cortex activity may be decreased in PD-VH vs PD-no-VH in response to more complex stimuli[31,32]. Similarly, previous resting state-work has described increased functional connectivity between superior, middle and inferior frontal gyri in PD-VH and occipital cortex[39]. An increased burden of Lewy-related pathology has also been reported in frontal cortex in PD-VH[13], as have grey matter reductions in the bilateral dorsolateral PFC[87].

The lateralised effect of PFC efferent connectivity we found is intriguing, in that we found increased top-down connectivity from left PFC to V1 and medial thalamus, but decreased top-down connectivity from right PFC to V1. Lateralised differences in prefrontal activity have also been reported in previous functional neuroimaging studies of PD-VH. Both

increased[76] and decreased[77] glucose metabolism have been observed in left PFC. Decreased right PFC BOLD activation has also been reported in PD-VH in response to faces[31], and just prior to presentation of complex stimuli[32]. Increased right PFC BOLD activation has meanwhile been reported in response to more simple stimuli[30]. A single-case study has also reported simultaneous activation of right medial frontal gyrus and deactivation of left middle frontal gyrus during active VH[88].

Asymmetry in lateral PFC influences have been shown in prediction error signalling in health, however right (rather than left) lateral PFC was implicated[16,17]. Our observation of increased effective connectivity from left PFC and decreased from right PFC is thus inconsistent with these findings. It is possible that Parkinson's disease disrupts the usual laterality of prediction error signals, though this needs to be tested in larger numbers of patients.

Although we found evidence to support the increased top-down and reduced bottom-up connectivity account of VH in Parkinson's disease, differences in effective connectivity between other regions are also implicated. For example, we also observed increased bottom-up connectivity from the left LGN and decreased top-down connectivity from right PFC in PD-VH, and this is further complicated by changes in regional self-connections. We found disinhibition of the left LGN (reduced intrinsic self-inhibition) which would be expected to amplify both the reduced bottom-up connectivity to medial thalamus and V1, and the increased bottom-up connectivity to left PFC. We further found disinhibition of the left PFC, which would amplify its increased top-down connections to medial thalamus and V1, and we found increased self-inhibition of right PFC, which would dampen its reduced top-down connection to V1. Of note, the combined differences in connectivity related to clinical measures of hallucination severity (both top 5 and top 10 connections) so a more complex shift in causal influences may be relevant. It is therefore important to consider the full set of changes in effective connectivity as well as both extrinsic and intrinsic connections when interpreting our results.

Limitations

One of the main limitations with the current paper is the relatively small number of PD-VH included. While similar sample sizes have been used in previous functional analyses of VH in Parkinson's disease[34,89], it will be important to examine effective connectivity in larger cohorts.

Patients in the current study continued their normal medication, including levodopa, during both clinical assessments and neuroimaging. This was done to avoid potential effects of distress and anxiety caused by omitting levodopa doses, which would affect cognitive function. Although we are not able to directly assess the effect of neurotransmitters on the current results, we note there was no significant difference in levodopa equivalent dose between hallucinators and non-hallucinators.

Additionally, while predicted group membership correlated significantly with actual group membership in our leave-one-out analysis, we were not able to predict group membership on a per-subject basis with high posterior probability. This could be explained by heterogeneity within the PD-no-VH group, whereby those who will go on to develop VH show a similar pattern to those who already have VH. However, longitudinal data would be needed to test this. That said, we did find that the pattern of connectivity was associated with hallucination severity within the PD-VH group.

Conclusions

Our spectral DCM analysis showed that VH in Parkinson's disease is associated with both reduced bottom-up and increased top-down effective connectivity within the visual network. This related particularly to intra-hemispheric connectivity to and from the LGN and PFC. The pattern of effective connectivity within the PD-VH group was significantly associated with the severity of their hallucinations. This study provides further evidence for the aberrant hierarchical predictive processing account of hallucinations in Parkinson's disease, and models resting state effective connectivity for the first time in this context.

FUNDING

GECT is supported by a PhD studentship from the Medical Research Council (Ref: MR/N013867/1). PZ is supported by core funding awarded by Wellcome, to the Wellcome Centre for Human Neuroimaging (Ref: 203147/Z/16/Z). AZ is supported by an Alzheimer's

Research UK Clinical Research Fellowship (Ref: 2018B-001). AR is supported by the Australian Research Council (Refs: DE170100128 and DP200100757) and Australian National Health and Medical Research Council Investigator Grant (Ref: 1194910). AR is also a CIFAR Azrieli Global Scholar in the Brain, Mind & Consciousness Program. RSW is supported by a Wellcome Clinical Research Career Development Fellowship (Ref: 205167/Z/16/Z). Recruitment to the study was also supported by Parkinson's UK, the Cure Parkinson's Trust. The study was further supported by UCLH Biomedical Research Centre Grant (Ref: BRC302/NS/RW/101410) and by grants from the National Institute for Health Research.

COMPETING INTERESTS

RSW has received honoraria from GE healthcare and Britannia.

FIGURE LEGENDS

Figure 1 – Within-subject dynamic causal modelling analysis. (A) Location of the eight nodes comprising the visual network used for all analyses (Dorsal, left-sagittal, and rostral views). **(B)** Timeseries extracted as the principal eigenvariate from each of the eight visual network nodes (example from a Parkinson's hallucinator, data from same patient shown for C and D) **(C)** Cross-spectral density plot, showing the frequency bands in which each of the eight regions were active. Real data are indicated by solid lines (and are second order statistics derived from the timeseries), while data estimated by the generative model are indicated by dashed lines. The variance explained by the model for this example subject is indicated in the top right. **(D)** Estimated connectivity parameters (connection strengths) for the eight regions, including 56 extrinsic (between-region) parameters, which are in hertz, and eight intrinsic (within-region) parameters indicated by dotted lines, which have a unitless log scale and modulate inherently negative self-connections. Error bars are 90% credible intervals derived from the posterior variance of each parameter. LGN = lateral geniculate nucleus; mThal. = medial thalamus; V1 = primary visual cortex; Hipp. = hippocampus; PFC = prefrontal cortex; DCM = dynamic causal model. Colour coding for regions is consistent across panels.

Figure 2 – Construction of factorial model space to test hypotheses about visual network hierarchical processing and architecture in Parkinson's disease with visual

hallucinations. Possible explanations for the data in the form of reduced models (i.e., some connections 'switched off' / restricted to their prior expectation of zero) were constructed based on their correspondence to three experimental factors for both the commonalities and differences between subjects.

Factor 1 examines top-down vs bottom-up connectivity and has 3 families within it: 1) – **Top-down:** bottom-up connections switched off, 2) – **Bottom-up:** top-down connections switched off and 3) – **Top-down and bottom-up:** no connections switched off.

Factor 2 examines inter- vs intra-hemispheric connectivity and has 3 families within it: 1) - **Inter-hemispheric:** intra-hemispheric connections switched off, 2) **Intra-hemispheric** inter-hemispheric connections switched off and 3) **Inter-hemispheric** and **Intra-hemispheric:** no connections switched off.

Factor 3 examines regional involvement and has 29 families within it, which were derived from all possible subsets of five bilateral regions (left and right LGN, medial thalamus, V1, left and right hippocampus, left and right PFC). For example, #1 all extrinsic connections switched off except those to and from the left and right PFC, #29 all extrinsic connections switched on except those specific to left and right PFC. All possible familial combinations across factors gave 3x3x29 = 261 possible models. After removal of duplicate models and addition of a null model with no connections switched on (including intrinsic ones), the final factorial model space contained 179 models each for the commonalities and differences between subjects. Therefore, 179^2 = 32041 possible hypotheses (PEB models) for the data were analysed.

Figure 3 – Bayesian model comparison across factorial model space gives possible explanations for visual network hierarchical processing and architecture.

(A) Joint posterior probability across all models. The axes list all 179 candidate models including the null model in terms of the commonalities across subjects and differences due to presence of visual hallucinations (i.e., the hypothesis in row *i* and column *j* had parameters relating to commonalities set according to model *i*, and parameters relating to presence of hallucinations set according to model *j*). The best model was number 172 (fully connected) for the commonalities and 143 (top-down and bottom-up with intra-hemispheric LGN and PGC) for differences, with 53% posterior probability.

(B) Summed posterior probability. The same result shown in panel A, summed over the columns to give the posterior probability for the commonalities across subjects, and summed over the rows and to give the posterior probability for the differences due to hallucinations.

(C) Spatial projections for the two single-best models described in panels A and B.

(D-F) Family analyses for each factor: D: top-down/bottom-up; E inter-/intra-hemispheric; F regional involvement.

Separate family analyses with the same 32041 hypothesis (reduced PEB models) from panel A grouped into different families. In each case, the element in row *m* and column *n* represents the pooled probability across models in which the commonalities parameters were set according to family *m* and the parameters relating to presence of hallucinations set according to family *n*. Factors and families are as described in Figure 2, and the probability associated with the null model is also plotted in each case.

Figure 4 – Bayesian model averaging across factorial model space gives magnitude of connection strengths across subjects, and differences associated with visual hallucinations. The Bayesian model average of parameter values across all 179 models for the commonalities between subjects and the differences between subjects due to the presence of visual hallucinations. All parameters are thresholded at posterior probability >95% of being present versus absent. **(A) Commonalities across all patients** (with and without hallucinations equivalent to the mean across subjects). Here, orange arrows / off-diagonal positive numbers reflect excitatory connectivity and blue arrows / off-diagonal negative numbers reflect inhibitory connectivity. Diagonal connectivity / self-connectivity is inhibitory by definition and is log-scale, hence leading diagonal positive numbers / orange spheres reflect more self-inhibition and leading diagonal negative numbers / blue spheres reflect disinhibition. **(B) Differences between hallucinators and non-hallucinators.** Here, orange arrows / off-diagonal positive numbers reflect increased connectivity in PD-VH versus PD-no-VH, whereas blue arrows / off-diagonal negative numbers reflect decreased connectivity. Leading diagonal positive numbers / orange spheres reflect increased self-inhibition in PD-VH versus PD-no-VH and leading diagonal negative numbers / blue spheres reflect increased disinhibition. LGN = Lateral geniculate nucleus; mTh = medial thalamus; Hipp. = hippocampus; PFC = prefrontal cortex.

Figure 5 – Visual network effective connectivity is associated with the presence and severity of visual hallucinations in Parkinson's disease.

(A) Results from leave-one-out cross validation across all 90 subjects. The five largest parameters in terms of overall group difference were used to predict the left-out subject's group membership. Correlation between predicted group effect and actual group effect, r is the Pearson's correlation coefficient.

(B) Relationship between differences in effective connectivity and hallucination severity. Results of canonical variate analysis for the 15 PD-VH. For each participant, the primary canonical variate derived from their individual values for the five largest parameters in terms of overall group difference between PD-VH and PD-no-VH is plotted against the primary canonical variate derived from their UMPDHQ score adjusted for age and sex, r is the Pearson's correlation coefficient.

REFERENCES

1. Fénelon G, Mahieux F, Huon R, Ziégler M. Hallucinations in Parkinson's disease. Prevalence, phenomenology and risk factors. *Brain*. 2000;123(4):733-745. doi:10.1093/brain/123.4.733

2. McKinlay A, Grace RC, Dalrymple-Alford JC, Anderson T, Fink J, Roger D. A profile of neuropsychiatric problems and their relationship to quality of life for Parkinson's disease patients without dementia. *Park Relat Disord*. 2008;14(1):37-42. doi:10.1016/j.parkreldis.2007.05.009

3. Goetz CG, Stebbins GT. Risk factors for nursing home placement in advanced parkinson's disease. *Neurology*. 1993;43(11):2227-2229. doi:10.1212/wnl.43.11.2227

4. Aarsland D, Larsen JP, Tandberg E, Laake K. Predictors of nursing home placement in Parkinson's disease: A population-based, prospective study. *J Am Geriatr Soc*. 2000;48(8):938-942. doi:10.1111/j.1532-5415.2000.tb06891.x

5. Galvin JE, Pollack J, Morris JC. Clinical phenotype of Parkinson disease dementia. *Neurology*. 2006;67(9):1605-1611. doi:10.1212/01.wnl.0000242630.52203.8f

6. Weil RS, Schrag AE, Warren JD, Crutch SJ, Lees AJ, Morris HR. Visual dysfunction in Parkinson's disease. *Brain*. 2016;139(11):2827-2843. doi:10.1093/brain/aww175

7. Powers AR, Kelley M, Corlett PR. Hallucinations as Top-Down Effects on Perception. *Biol Psychiatry Cogn Neurosci Neuroimaging*. 2016;1(5):393-400.

doi:10.1016/j.bpsc.2016.04.003

8. Corlett PR, Horga G, Fletcher PC, Alderson-Day B, Schmack K, Powers AR. Hallucinations and Strong Priors. *Trends Cogn Sci*. 2019;23(2):114-127. doi:10.1016/j.tics.2018.12.001

9. Price MJ, Feldman R, Adelberg D, Kayne H. Abnormalities in color vision and contrast sensitivity in parkinson's disease. *Neurology*. 1992;42(4):887-890. doi:10.1212/wnl.42.4.887

10. Anang JBM, Gagnon JF, Bertrand JA, et al. Predictors of dementia in Parkinson disease: A prospective cohort study. *Neurology*. 2014;83(14):1253-1260. doi:10.1212/WNL.0000000000000842

11. Leyland L-A, Bremner FD, Mahmood R, et al. Visual tests predict dementia risk in Parkinson's disease. *Neurol Clin Pract*. 2019;In Press.

12. Zarkali A, McColgan P, Leyland LA, Lees AJ, Weil RS. Visual Dysfunction Predicts Cognitive Impairment and White Matter Degeneration in Parkinson's Disease. *Mov Disord*. 2021;36(5):1191-1202. doi:10.1002/mds.28477

13. Gallagher DA, Parkkinen L, O'Sullivan SS, et al. Testing an aetiological model of visual hallucinations in Parkinson's disease. *Brain*. 2011;134(11):3299-3309. doi:10.1093/brain/awr225

14. O'Callaghan C, Hall JM, Tomassini A, et al. Visual Hallucinations Are Characterized by Impaired Sensory Evidence Accumulation: Insights From Hierarchical Drift Diffusion Modeling in Parkinson's Disease. *Biol Psychiatry Cogn Neurosci Neuroimaging*. 2017;2(8):680-688. doi:10.1016/j.bpsc.2017.04.007

15. Zarkali A, Adams RA, Psarras S, Leyland L-A, Rees G, Weil RS. Increased weighting on prior knowledge in Lewy body-associated visual hallucinations. *Brain Commun*. 2019;1(1):1-13. doi:10.1093/braincomms/fcz007

16. Fletcher PC, Anderson JM, Shanks DR, et al. Responses of human frontal cortex to surprising events are predicted by formal associative learning theory. *Nat Neurosci*. 2001;4(10):1043-1048. doi:10.1038/nn733

17. Corlett PR, Aitken MRF, Dickinson A, et al. Prediction error during retrospective revaluation of causal associations in humans: fMRI evidence in favor of an associative

model of learning. *Neuron*. 2004;44(5):877-888. doi:10.1016/j.neuron.2004.11.022

18. McCormick DA, McGinley MJ, Salkoff DB. Brain state dependent activity in the cortex and thalamus. *Curr Opin Neurobiol*. 2015;31:133-140. doi:10.1016/j.conb.2014.10.003

19. Shine JM. The thalamus integrates the macrosystems of the brain to facilitate complex, adaptive brain network dynamics. *Prog Neurobiol*. 2021;199:101951. doi:10.1016/j.pneurobio.2020.101951

20. Zarkali A, McColgan P, Leyland LA, Lees AJ, Weil RS. Longitudinal thalamic white and grey matter changes associated with visual hallucinations in Parkinson's disease. *J Neurol Neurosurg Psychiatry*. 2022;93(2):169-179. doi:10.1136/jnnp-2021-326630

21. Weil RS, Hsu JK, Darby RR, Soussand L, Fox MD. Neuroimaging in Parkinson's disease dementia: connecting the dots. *Brain Commun*. 2019;1(1). doi:10.1093/braincomms/fcz006

22. Kim NY, Hsu J, Talmasov D, et al. Lesions causing hallucinations localize to one common brain network. *Mol Psychiatry*. 2021;26(4):1299-1309. doi:10.1038/s41380-019-0565-3

23. Behrendt RP. Contribution of hippocampal region CA3 to consciousness and schizophrenic hallucinations. *Neurosci Biobehav Rev*. 2010;34(8):1121-1136. doi:10.1016/j.neubiorev.2009.12.009

24. Goodale MA, Milner AD. Separate visual pathways for perception and action. *Trends Neurosci*. 1992;15(1):20-25. doi:10.1016/0166-2236(92)90344-8

25. Harding AJ, Broe GA, Halliday GM. Visual hallucinations in Lewy body disease relate to Lewy bodies in the temporal lobe. *Brain*. 2002;125(2):391-403. doi:10.1093/brain/awf033

26. Yao N, Cheung C, Pang S, et al. Multimodal MRI of the hippocampus in Parkinson's disease with visual hallucinations. *Brain Struct Funct*. 2016;221(1):287-300. doi:10.1007/s00429-014-0907-5

27. Pezzoli S, Cagnin A, Bandmann O, Venneri A. Structural and functional neuroimaging of visual hallucinations in lewy body disease: A systematic literature review. *Brain Sci*. 2017;7(7):1-32. doi:10.3390/brainsci7070084

28. Stebbins GT, Goetz GG, Carrillo MC, et al. Altered cortical visual processing in PD with hallucinations: An fMRI study. *Neurology*. 2004;63(8):1409-1416. doi:10.1212/01.WNL.0000141853.27081.BD

29. Holroyd S, Wooten GF. Preliminary fMRI Evidence of Visual System Dysfunction in Parkinson's Disease Patients With Visual Hallucinations. *J Neuropsychiatr*. 2006;18(3):402-404. doi:10.1176/appi.neuropsych.18.3.402

30. Lefebvre S, Baille G, Jardri R, et al. Hallucinations and conscious access to visual inputs in Parkinson's disease. *Sci Rep*. 2016;6(June):1-10. doi:10.1038/srep36284

31. Ramírez-Ruiz B, Martí MJ, Tolosa E, et al. Brain response to complex visual stimuli in Parkinson's patients with hallucinations: A functional magnetic resonance imaging study. *Mov Disord*. 2008;23(16):2335-2343. doi:10.1002/mds.22258

32. Meppelink AM, de Jong BM, Renken R, Leenders KL, Cornelissen FW, van Laar T. Impaired visual processing preceding image recognition in Parkinson's disease patients with visual hallucinations. *BRAIN*. 2009;132:2980-2993. doi:10.1093/brain/awp223

33. Shine JM, Muller AJ, O'Callaghan C, Hornberger M, Halliday GM, Lewis SJG. Abnormal connectivity between the default mode and the visual system underlies the manifestation of visual hallucinations in Parkinson's disease: A task-based fMRI study. *Parkinsons Dis*. 2015;1(December 2014). doi:10.1038/npjparkd.2015.3

34. Yao N, Shek-Kwan Chang R, Cheung C, et al. The Default Mode Network is Disrupted in Parkinson's Disease with Visual Hallucinations. *Hum Brain Mapp*. 2014;35(11):5658-5666. doi:10.1002/hbm.22577

35. Franciotti R, Delli Pizzi S, Perfetti B, et al. Default mode network links to visual hallucinations: A comparison between Parkinson's disease and multiple system atrophy. *Mov Disord*. 2015;30(9):1237-1247. doi:10.1002/mds.26285

36. Shine JM, Keogh R, O'Callaghan C, Muller AJ, Lewis SJG, Pearson J. Imagine that: Elevated sensory strength of mental imagery in individuals with Parkinson's disease and visual hallucinations. *Proc R Soc B Biol Sci*. 2015;282(1798). doi:10.1098/rspb.2014.2047

37. Dujardin K, Roman D, Baille G, et al. What can we learn from fMRI capture of visual

hallucinations in Parkinson's disease? *Brain Imaging Behav*. 2020;14(2):329-335. doi:10.1007/s11682-019-00185-6

38. Walpola IC, Muller AJ, Hall JM, et al. Mind-wandering in Parkinson's disease hallucinations reflects primary visual and default network coupling. *Cortex*. 2020;125:233-245. doi:10.1016/j.cortex.2019.12.023

39. Yao N, Pang S, Cheung C, et al. Resting activity in visual and corticostriatal pathways in Parkinson's disease with hallucinations. *Park Relat Disord*. 2015;21(2):131-137. doi:10.1016/j.parkreldis.2014.11.020

40. Bejr-kasem H, Pagonabarraga J, Martínez-Horta S, et al. Disruption of the default mode network and its intrinsic functional connectivity underlies minor hallucinations in Parkinson's disease. *Mov Disord*. 2019;34(1):78-86. doi:10.1002/mds.27557

41. Friston KJ, Kahan J, Biswal B, Razi A. A DCM for resting state fMRI. *Neuroimage*. 2014;94:396-407. doi:10.1016/j.neuroimage.2013.12.009

42. Zeidman P, Jafarian A, Corbin N, et al. A guide to group effective connectivity analysis, part 1: First level analysis with DCM for fMRI. *Neuroimage*. 2019;200(May):174-190. doi:10.1016/j.neuroimage.2019.06.031

43. Li B, Daunizeau J, Stephan KE, Penny W, Hu D, Friston K. Generalised filtering and stochastic DCM for fMRI. *Neuroimage*. 2011;58(2):442-457. doi:10.1016/j.neuroimage.2011.01.085

44. Razi A, Kahan J, Rees G, Friston KJ. Construct validation of a DCM for resting state fMRI. *Neuroimage*. 2015;106:1-14. doi:10.1016/j.neuroimage.2014.11.027

45. Gibb WRG, Lees AJ. The relevance of the Lewy body to the pathogenesis of idiopathic Parkinson's disease. *J Neurol Neurosurg Psychiatry*. 1988;51(6):745-752. doi:10.1136/jnnp.51.6.745

46. Goetz CG, Tilley BC, Shaftman SR, et al. Movement Disorder Society-sponsored revision of the Unified Parkinson's Disease Rating Scale (MDS-UPDRS): Scale presentation and clinimetric testing results. *Mov Disord*. 2008;23(15):2129-2170. doi:10.1002/mds.22340

47. Nasreddine ZS, Phillips NA, Bédirian V, et al. The Montreal Cognitive Assessment, MoCA: A brief screening tool for mild cognitive impairment. *J Am Geriatr Soc*.

2005;53(4):695-699. doi:10.1111/j.1532-5415.2005.53221.x

48. Sloan LL. New test charts for the measurement of visual acuity at far and near distances. *Am J Ophthalmol*. 1959;48(6):807-813. doi:10.1016/0002-9394(59)90626-9

49. Hummel T, Sekinger B, Wolf SR, Pauli E, Kobal G. “Sniffin” sticks’. Olfactory performance assessed by the combined testing of odor identification, odor discrimination and olfactory threshold. *Chem Senses*. 1997;22(1):39-52. doi:10.1093/chemse/22.1.39

50. Zigmond AS, Snaith RP. The Hospital Anxiety and Depression Scale. *Acta Psychiatr Scand*. 1983;67(6):361-370. doi:10.1111/j.1600-0447.1983.tb09716.x

51. Stiasny-Kolster K, Mayer G, Schäfer S, Möller JC, Heinzel-Gutenbrunner M, Oertel WH. The REM sleep behavior disorder screening questionnaire - A new diagnostic instrument. *Mov Disord*. 2007;22(16):2386-2393. doi:10.1002/mds.21740

52. Tomlinson CL, Stowe R, Patel S, Rick C, Gray R, Clarke CE. Systematic review of levodopa dose equivalency reporting in Parkinson’s disease. *Mov Disord*. 2010;25(15):2649-2653. doi:10.1002/mds.23429

53. Papapetropoulos S, Katzen H, Schrag A, et al. A questionnaire-based (UM-PDHQ) study of hallucinations in Parkinson’s disease. *BMC Neurol*. 2008;8:1-8. doi:10.1186/1471-2377-8-21

54. Esteban O, Birman D, Schaer M, Koyejo OO, Poldrack RA, Gorgolewski KJ. MRIQC: Advancing the automatic prediction of image quality in MRI from unseen sites. *PLoS One*. Published online 2017. doi:10.1371/journal.pone.0184661

55. Parkes L, Fulcher BD, Yücel M, Fornito A. An evaluation of the efficacy, reliability, and sensitivity of motion correction strategies for resting-state functional MRI. *Neuroimage*. 2018;171(July 2017):415-436. doi:10.1016/j.neuroimage.2017.12.073

56. Pruim RHR, Mennes M, van Rooij D, Llera A, Buitelaar JK, Beckmann CF. ICA-AROMA: A robust ICA-based strategy for removing motion artifacts from fMRI data. *Neuroimage*. 2015;112:267-277. doi:10.1016/j.neuroimage.2015.02.064

57. Pruim RHR, Mennes M, Buitelaar JK, Beckmann CF. Evaluation of ICA-AROMA and alternative strategies for motion artifact removal in resting state fMRI. *Neuroimage*. 2015;112:278-287. doi:10.1016/J.NEUROIMAGE.2015.02.063

58. Kalaitzakis ME, Christian LM, Moran LB, Graeber MB, Pearce RKB, Gentleman SM. Dementia and visual hallucinations associated with limbic pathology in Parkinson's disease. *Park Relat Disord*. 2009;15(3):196-204. doi:10.1016/j.parkreldis.2008.05.007

59. Paneri S, Gregoriou GG. Top-down control of visual attention by the prefrontal cortex. Functional specialization and long-range interactions. *Front Neurosci*. 2017;11(SEP):1-16. doi:10.3389/fnins.2017.00545

60. Wolff M, Vann SD. The cognitive thalamus as a gateway to mental representations. *J Neurosci*. 2019;39(1):3-14. doi:10.1523/JNEUROSCI.0479-18.2018

61. Iglesias JE, Augustinack JC, Nguyen K, et al. A computational atlas of the hippocampal formation using ex vivo, ultra-high resolution MRI: Application to adaptive segmentation of in vivo MRI. *Neuroimage*. 2015;115:117-137. doi:10.1016/j.neuroimage.2015.04.042

62. Iglesias JE, Insausti R, Lerma-Usabiaga G, et al. A probabilistic atlas of the human thalamic nuclei combining ex vivo MRI and histology. *Neuroimage*. 2018;183(August):314-326. doi:10.1016/j.neuroimage.2018.08.012

63. Razi A, Seghier ML, Zhou Y, Mccolgan P, Zeidman P. Large-scale DCMs for resting-state fMRI. 2018;1(3):222-241. doi:10.1162/NETN

64. Thomas Yeo BT, Krienen FM, Sepulcre J, et al. The organization of the human cerebral cortex estimated by intrinsic functional connectivity. *J Neurophysiol*. 2011;106(3):1125-1165. doi:10.1152/jn.00338.2011

65. Friston K, Mattout J, Trujillo-Barreto N, Ashburner J, Penny W. Variational free energy and the Laplace approximation. *Neuroimage*. 2007;34(1):220-234. doi:10.1016/j.neuroimage.2006.08.035

66. Friston KJ, Litvak V, Oswal A, et al. Bayesian model reduction and empirical Bayes for group (DCM) studies. *Neuroimage*. 2016;128:413-431. doi:10.1016/j.neuroimage.2015.11.015

67. Penny WD, Mattout J, Trujillo-Barreto N. Bayesian model selection and averaging. In: *Statistical Parametric Mapping: The Analysis of Functional Brain Images*. ; 2007:454-467. doi:10.1016/B978-012372560-8/50035-8

68. Friston K, Penny W. Post hoc Bayesian model selection. *Neuroimage*.

2011;56(4):2089-2099. doi:10.1016/j.neuroimage.2011.03.062

69. Rosa MJ, Friston K, Penny W. Post-hoc selection of dynamic causal models. *J Neurosci Methods*. 2012;208(1):66-78. doi:10.1016/j.jneumeth.2012.04.013

70. Xia M, Wang J, He Y. BrainNet Viewer: A Network Visualization Tool for Human Brain Connectomics. *PLoS One*. 2013;8(7). doi:10.1371/journal.pone.0068910

71. Kass RE, Raftery AE. Bayes factors. *J Am Stat Assoc*. 1995;90(430):773-795. doi:10.1080/01621459.1995.10476572

72. Penny WD, Stephan KE, Mechelli A, Friston KJ. Comparing dynamic causal models. *Neuroimage*. 2004;22(3):1157-1172. doi:10.1016/j.neuroimage.2004.03.026

73. Razi A, Friston KJ. The Connected Brain: Causality, models, and intrinsic dynamics. *IEEE Signal Process Mag*. 2016;33(3):14-55. doi:10.1109/MSP.2015.2482121

74. Lenka A, Jhunjhunwala KR, Saini J, Pal PK. Structural and functional neuroimaging in patients with Parkinson's disease and visual hallucinations: A critical review. *Park Relat Disord*. 2015;21(7):683-691. doi:10.1016/j.parkreldis.2015.04.005

75. Firbank MJ, Parikh J, Murphy N, et al. Reduced occipital GABA in Parkinson disease with visual hallucinations. *Neurology*. 2018;91(7):e675. doi:10.1212/WNL.0000000000006007

76. Nagano-Saito A, Washimi Y, Arahata Y, et al. Visual hallucination in Parkinson's disease with FDG PET. *Mov Disord*. 2004;19(7):801-806. doi:10.1002/mds.20129

77. Boecker H, Ceballos-Baumann AO, Volk D, Conrad B, Forstl H, Haussermann P. Metabolic alterations in patients with Parkinson disease and visual hallucinations. *Arch Neurol*. 2007;64(7):984-988. doi:10.1001/archneur.64.7.984

78. Bellot E, Kauffmann L, Coizet V, Meoni S, Moro E, Dojat M. Effective connectivity in subcortical visual structures in de novo Patients with Parkinson's Disease. *NeuroImage Clin*. 2022;33:102906. doi:10.1016/j.nicl.2021.102906

79. Moro E, Bellot E, Meoni S, et al. Visual Dysfunction of the Superior Colliculus in De Novo Parkinsonian Patients. *Ann Neurol*. 2020;87(4):533-546. doi:10.1002/ana.25696

80. Delli Pizzi S, Franciotti R, Tartaro A, et al. Structural alteration of the dorsal visual network in DLB patients with visual hallucinations: A cortical thickness MRI study.

PLoS One. 2014;9(1):1-7. doi:10.1371/journal.pone.0086624

81. Matar E, Brooks D, Lewis SJG, Halliday GM. Limbic thalamus atrophy is associated with visual hallucinations in Lewy body disorders. *Neurobiol Aging*. 2022;112:122-128. doi:10.1016/J.NEUROBIOLAGING.2022.01.001

82. Kosciessa JQ, Lindenberger U, Garrett DD. Thalamocortical excitability modulation guides human perception under uncertainty. *Nat Commun*. 2021;12(1). doi:10.1038/s41467-021-22511-7

83. Mukherjee A, Lam NH, Wimmer RD, Halassa MM. Thalamic circuits for independent control of prefrontal signal and noise. *Nature*. 2021;600(7887):100-104. doi:10.1038/s41586-021-04056-3

84. Müller F, Lenz C, Dolder P, et al. Increased thalamic resting-state connectivity as a core driver of LSD-induced hallucinations. *Acta Psychiatr Scand*. 2017;136(6):648-657. doi:10.1111/acps.12818

85. Preller KH, Razi A, Zeidman P, Stämpfli P, Friston KJ, Vollenweider FX. Effective connectivity changes in LSD-induced altered states of consciousness in humans. *Proc Natl Acad Sci U S A*. 2019;116(7):2743-2748. doi:10.1073/pnas.1815129116

86. Stoliker D, Egan GF, Friston KJ, Razi A. Neural Mechanisms and Psychology of Psychedelic Ego Dissolution. *PsyArXiv*. 2021;[preprint]. doi:10.31234/OSF.IO/AEWTM

87. Watanabe H, Senda J, Kato S, et al. Cortical and subcortical brain atrophy in Parkinson's disease with visual hallucination. *Mov Disord*. 2013;28(12):1732-1736. doi:10.1002/mds.25641

88. Goetz CG, Vaughan CL, Goldman JG, Stebbins GT. I finally see what you see: Parkinson's disease visual hallucinations captured with functional neuroimaging. *Mov Disord*. 2014;29(1):115-117. doi:10.1002/mds.25554

89. Hepp DH, Foncke EMJ, Dubbelink KTEO, Berg WDJV De, Berendse HW, Schoonheim MM. Loss of functional connectivity in patients with Parkinson disease and visual hallucinations. *Radiology*. 2017;285(3):896-903. doi:10.1148/radiol.2017170438

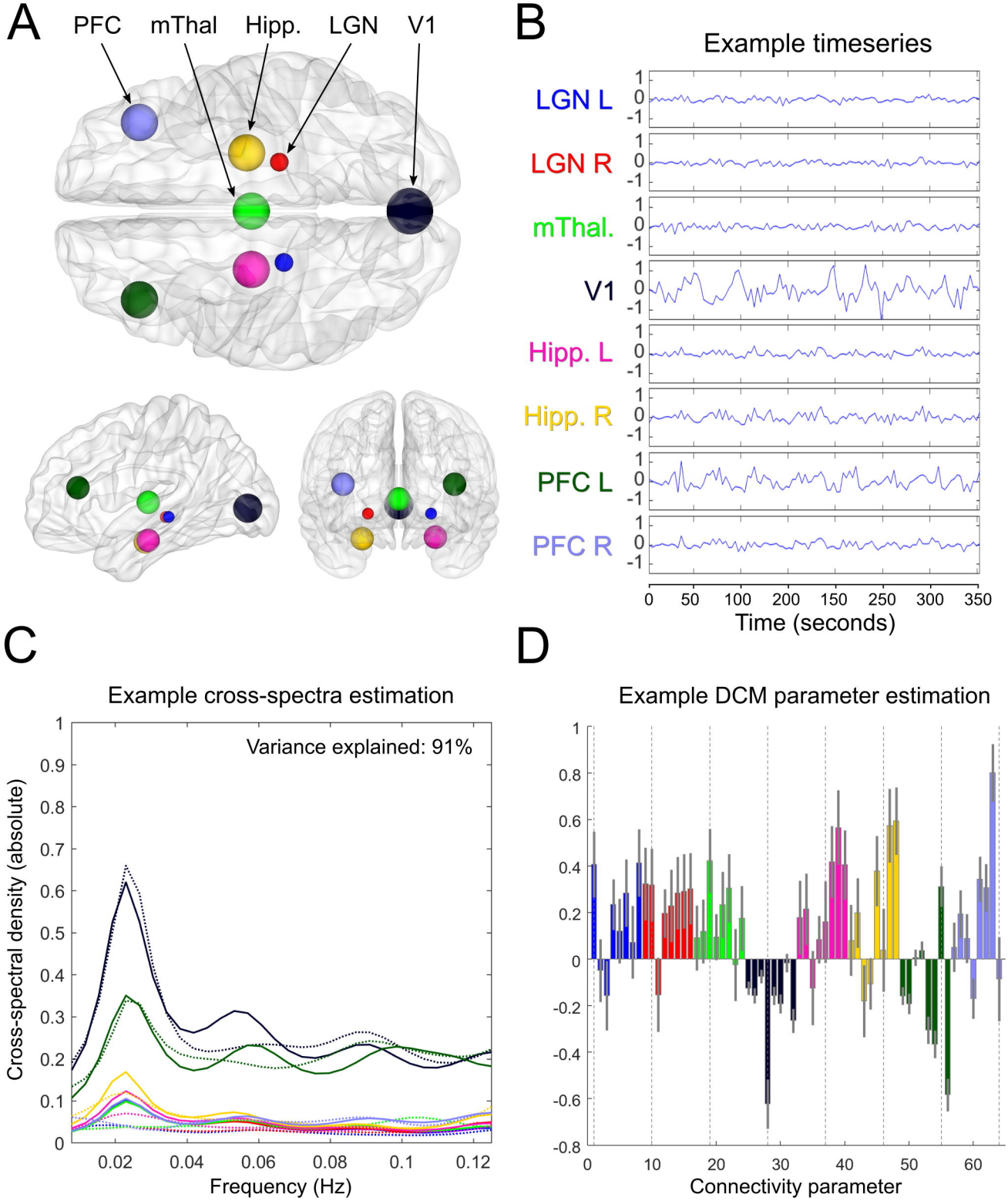
A
PFC
mThal
Hipp.
LGN
V1
B
Example timeseries
LGN L
LGN R
mThal.
V1
Hipp. L
Hipp. R
PFC L
PFC R
1
0
-1
0
50
100
200
150
250
300
350
Time (seconds)
C
Example cross-spectra estimation
Variance explained: 91%
Cross-spectral density (absolute)
Frequency (Hz)
0.02
0.04
0.06
0.08
0.1
0.12
D
Example DCM parameter estimation
Connectivity parameter

FACTOR 1: TOP-DOWN / BOTTOM-UP CONNECTIONS

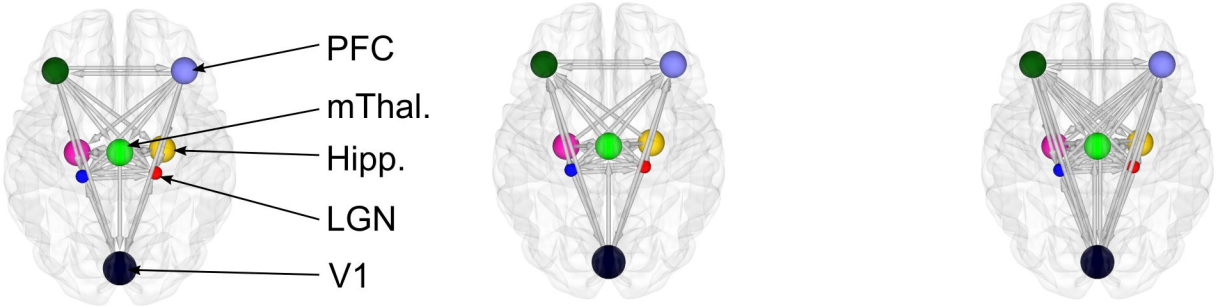

Top-down
#1

Bottom-up
#2

Top-down & bottom-up
#3

FACTOR 2: INTER- / INTRA-HEMISPHERIC CONNECTIONS

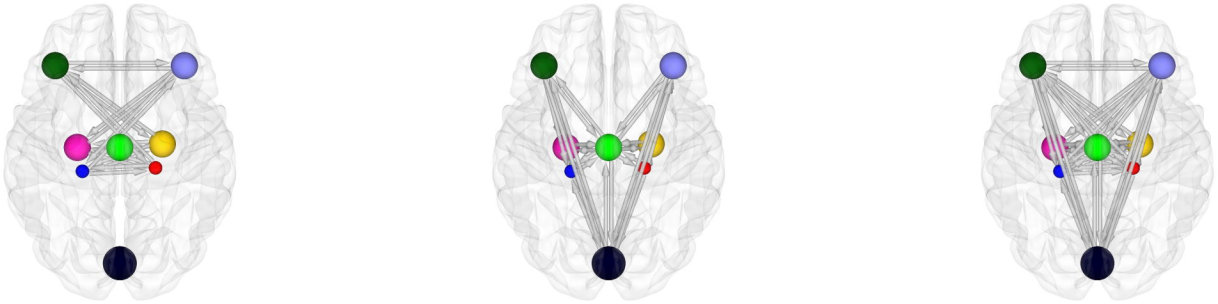

Inter-hemispheric
#1

Intra-hemispheric
#2

Inter- & intra-hemspheric
#3

FACTOR 3: REGIONAL INVOLVEMENT

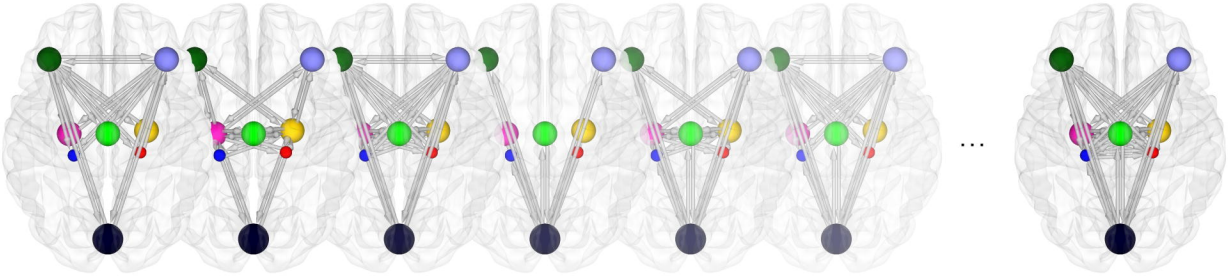

PFC
#1

Hipp.
#2

Hipp. & PFC
#3

V1
#4

V1 & Hipp.
#5

V1 & PFC
#6

...

...

LGN, mThal, V1 & Hipp.
#29

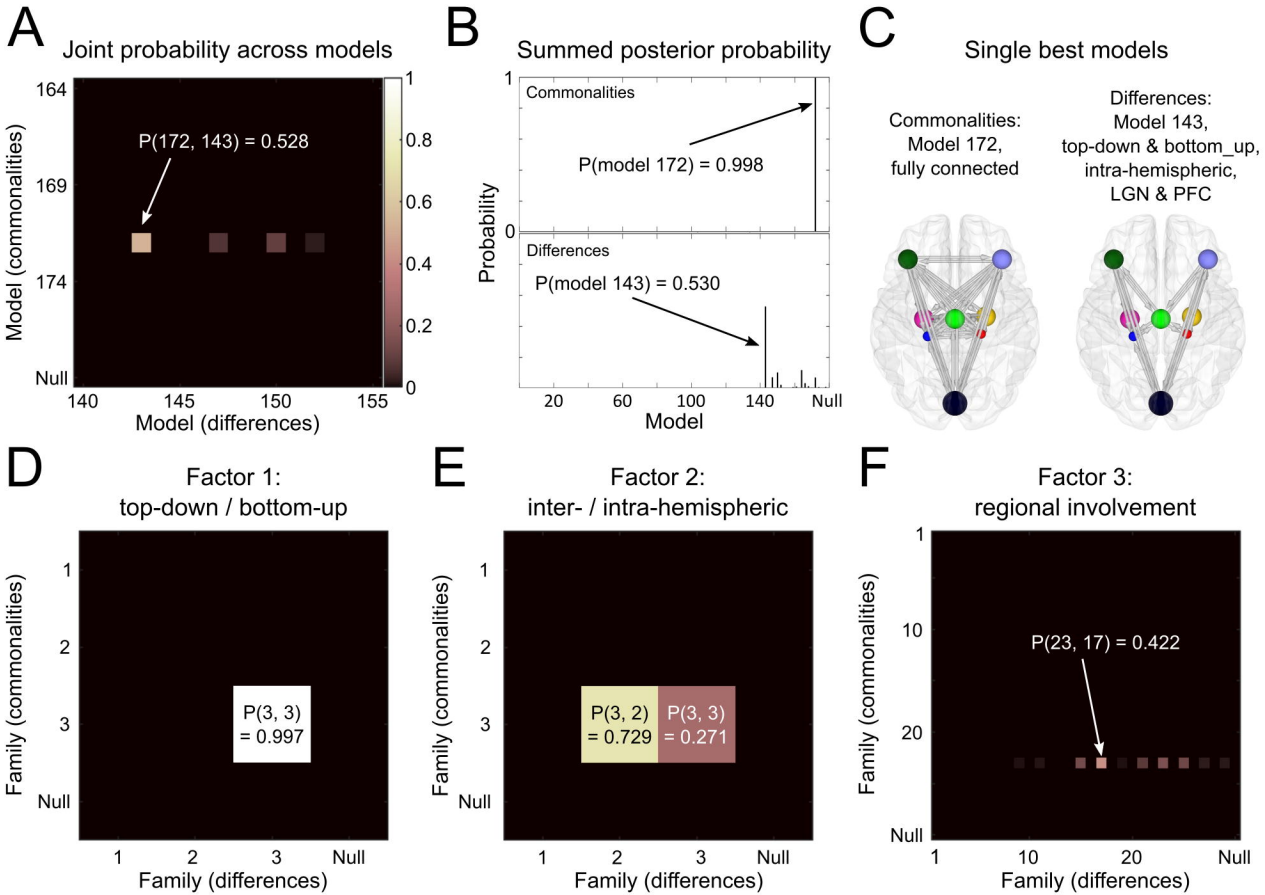
A
Joint probability across models
P(172, 143) = 0.528
Model (commonalities)
164
169
174
Null
140
145
150
155
Model (differences)
1
0.8
0.6
0.4
0.2
0
B
Summed posterior probability
Commonalities
P(model 172) = 0.998
Differences
P(model 143) = 0.530
Probability
1
0
20
60
100
140
Null
Model
C
Single best models
Commonalities:
Model 172,
fully connected
Differences:
Model 143,
top-down & bottom_up,
intra-hemispheric,
LGN & PFC
D
Factor 1:
top-down / bottom-up
P(3, 3)
= 0.997
Family (commonalities)
1
2
3
Null
Family (differences)
E
Factor 2:
inter- / intra-hemispheric
P(3, 2)
= 0.729
P(3, 3)
= 0.271
F
Factor 3:
regional involvement
P(23, 17) = 0.422
10
20

A. Commonalities across subjects

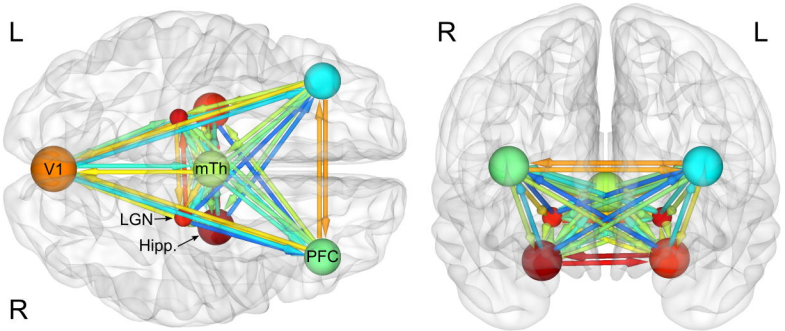

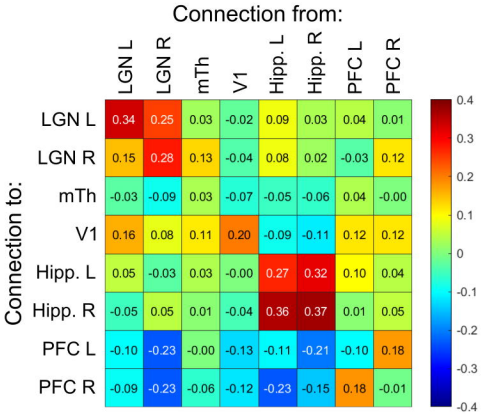

B. Differences due to VH

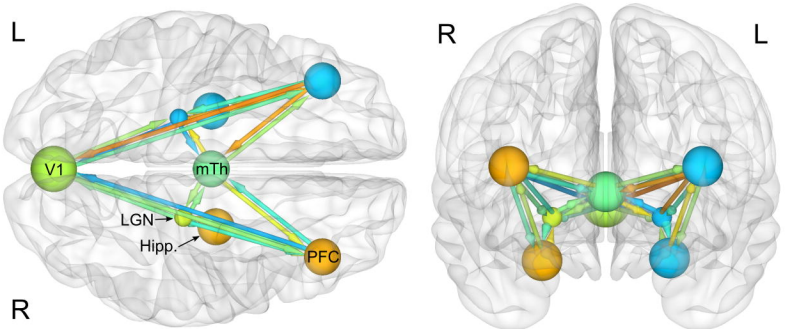

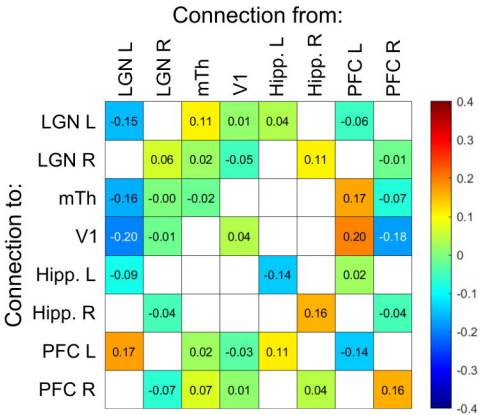

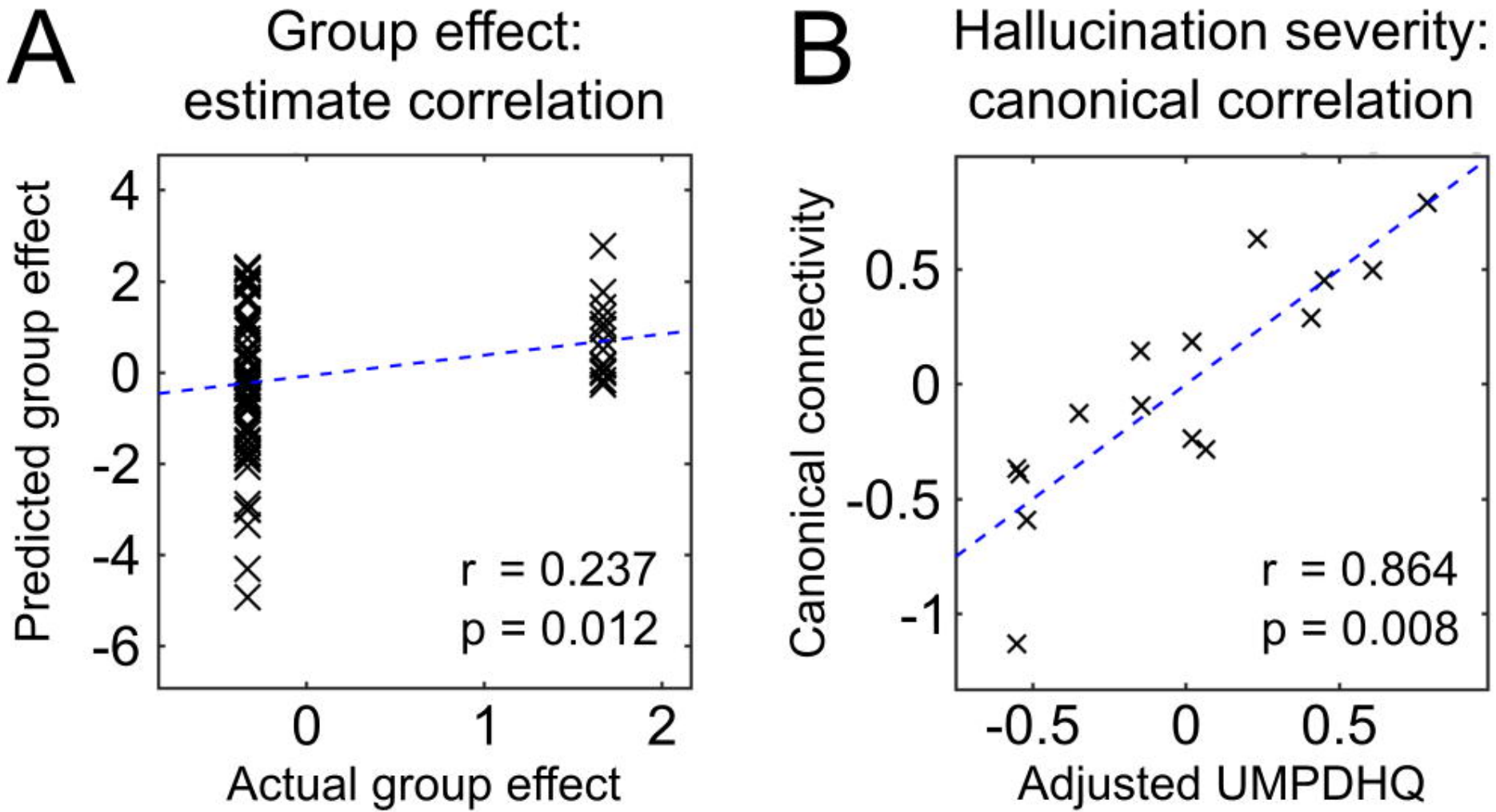
A
Group effect:
estimate correlation
Predicted group effect
4
2
0
-2
-4
-6
0
1
2
Actual group effect
r = 0.237
p = 0.012
B
Hallucination severity:
canonical correlation
Canonical connectivity
0.5
0
-0.5
-1
-0.5
0
0.5
Adjusted UMPDHQ
r = 0.864
p = 0.008